DOI: 10.1021/ma902566h

Macromolecules
ARTICLE

Temperature and Molecular Weight Dependent Hierarchical Equilibrium Structures in Semiconducting Poly(3-hexylthiophene)

Zhiyong Wu,[†] Albrecht Petzold,[†] Thomas Henze,[†] Thomas Thurn-Albrecht,*[,†] Ruth H. Lohwasser,[‡] Michael Sommer,[‡] and Mukundan Thelakkat*[,‡]

[†]*Institut für Physik, Martin-Luther-Universität Halle-Wittenberg, 06099 Halle, Germany, and* [‡]*Angewandte Funktionspolymere, Makromolekulare Chemie I, Universität Bayreuth, 95440 Bayreuth, Germany*

Received November 24, 2009; Revised Manuscript Received April 16, 2010

ABSTRACT: We report on structural investigations of a series of regioregular poly(3-hexylthiophene) with well-defined molecular weight (5−19 kg/mol) using DSC, small angle and wide-angle X-ray scattering, and AFM. With increasing temperature, we identify three ordered phases, namely 3D crystalline, 2D crystalline with disordered side chains, and a layered phase of smectic symmetry, followed by complete melting. Although all samples crystallize in extended chain conformation, the lower molecular weight material exhibits a lower crystallinity, most likely caused by noncrystallizable end groups. The crystallinity increases strongly with increasing molecular weight, which could be a possible explanation for the known dependence of charge transport properties on molecular weight.

Introduction

Semiconductor conjugated polymers have attracted widespread scientific interest triggered by their potential applications in electronic devices like solar cells, light emitting diodes or field effect transistors.[1−4] The steady increase in material performance parameters as, e.g., charge carrier mobility over the last 2 decades has brought these applications closer to reality. Devices based on organic materials and especially solvent processable polymers have potential advantages such as low cost, light weight, and flexibility compared to those made from inorganic semiconductors. Compared to low molecular weight materials, polymers in general tend to be more disordered and to exhibit a complex, hierarchical microstructure. Even chemically very regular, crystallizable polymers form usually only semicrystalline materials and display a crystalline−amorphous superstructure on a scale comparable to the size of the chain,[5] a fact which should be of relevance especially for charge transport.

Because of their high mobility poly(3-hexylthiophene) (P3HT) and other polythiophenes belong to the most promising polymers for optoelectronic applications.[6−8] With their relatively stiff main chain[9] to which flexible alkyl side chains are attached in order to increase solubility, they generally develop layered crystalline structures with separated main and side chains. $\pi-\pi$ stacking of planar backbones leads to delocalization of electronic states across different chains.[10] The crystalline structure of P3HT has been studied at several instances, in the initial reports an orthorhombic unit cell as schematically depicted in Figure 1 was reported.[11−14] More recent investigations find slight deviations and monoclinic unit cells are suggested.[15,16] As mentioned, a full description of the structure of P3HT requires further elements. First there is the question about the order and the dynamic state of the side chains. While originally a well ordered arrangement of side chains tilted with respect to the main chain without interdigitation was proposed,[13] there is no complete agreement about this point in the literature and recently Kline et al. concluded from spectroscopic experiments that the side chains are disordered at room temperature.[13,17−19] There is some evidence, mostly from DSC data, that at elevated temperatures a separate side chain melting can occur,[14,20−23] but the results are less clear for P3HT than for poly(3-alkylthiophenes) with longer side chains. Also there is no conclusive set of complementary calorimetric and structure analysis experiments. Upon crystallization, polymers generally form lamellar crystals separated by amorphous layers, the same is true for P3HT.[24] As additional parameters the thicknesses of the crystalline and amorphous layers d_c and d_a are therefore needed to describe the full structure (cf. Figure 1). The amorphous part can contain folds or other topological defects but also chemical defects like noncrystallizable comonomers or in case of P3HT regiodefects. Generally, for polymers the melting temperature depends on the crystal thickness. As a special characteristic, P3HT adapts a layered phase of smectic symmetry at elevated temperatures in between the crystalline and the isotropic phase. In this phase the separation

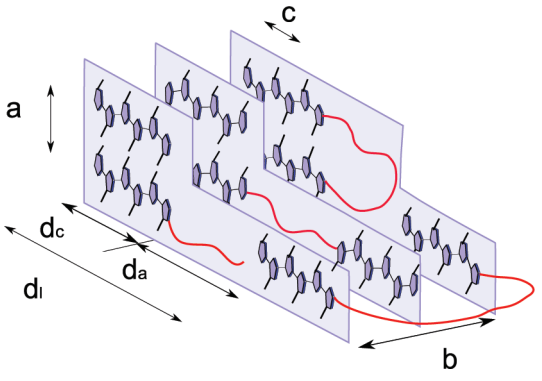

Figure 1. Scheme of the typical microstructure of regioregular P3HT. Key: ***a***, ***b***, ***c***, crystal lattice parameters; d_c, thickness of lamellar crystals; d_a, thickness of amorphous layers, d_l, long period, $d_l = d_a + d_c$ (scheme not to scale: the long period d_l is about on order of magnitude larger than the lattice parameters ***a***, ***b***, ***c***).

*To whom correspondence should be addressed. E-mail: (T.T.-A.) thomas.thurn-albrecht@physik.uni-halle.de; (M.T.) mukundan.thelakkat@uni-bayreuth.de.

 Published on Web 04/27/2010

between main and side chains remains intact.[25] Given the complex phase diagram of P3HT, the thermal history as well as the exact chemical structure can be decisive for the formation of a special morphology. The design of annealing procedures has to be based on the temperature dependent phase diagram, as the molecular mobility in the different phases is largely different.[25]

Given the fact that electronic transport properties are typically much more favorable in highly ordered, crystalline materials than in amorphous disordered materials, it is clear that the properties of polymer electronic devices will heavily depend on the extent to which structure and morphology of the corresponding materials can be controlled.[26] An exemplary yet ambiguous current debate in this context concerns the molecular weight dependence of the charge carrier mobility of regioregular P3HT in thin films, as measured in an OFET device. With increasing molecular weight the charge carrier mobility increases and the absorption spectrum shows a red shift.[27−31] On the structural side the observations are less clear. While the long period and presumably the crystal thickness as observed by AFM and GISAXS increases with molecular weight, experiments also seem to indicate that the amount of order decreases with increasing molecular weight. AFM images show a small scale nodular structure as opposed to a lamellar structure and Bragg intensities in X-ray diffraction experiments become weaker for higher molecular weight. Several possible explanations are proposed to solve the obvious discrepancies. While Kline et al. attributed the higher mobility in high molecular weight materials to a higher interconnectivity of the crystalline network,[28] Neher et al. on the other hand suggested that the correlation between mobility and molecular weight is related to a larger distortion of the backbone in the low molecular weight materials.[31] On the basis of the recent observation that the crystallinity and the melting temperature of P3HT increase with increasing molecular weight,[32] the same authors recently suggested that the transport properties are largely determined by the crystallinity of the samples. Somewhat in contradiction Brinkmann et al. found by electron microscopy that the thickness of crystalline lamellae is independent of the molecular weight.[33]

We here report on a study of a series of chemically well-defined P3HT samples with high regioregularity and narrow molecular weight distribution, using a combination of different experimental techniques (DSC, SAXS, WAXS, AFM) in order to determine the temperature and molecular weight dependent equilibrium crystal structure and morphology in bulk. While technologically often thin film samples are relevant, we here on purpose start with a study of bulk samples as a basis from which additional interfacial effects can be understood. We contribute to a clarification of some of the open questions mentioned above, concerning state and structure of the side chains, the occurrence of a separate side chain melting transition, and the molecular weight dependence of the morphology for low and intermediate molecular weight, i.e. the range which is most probably of practical relevance. While we do not address the mobility problem directly, we believe that our results should hold at least qualitatively in general and should be of relevance for a basic understanding and optimization of the electronic properties of P3HT.

Experiments

DSC. A Diamond differential scanning calorimeter from Perkin-Elmer was used to investigate the thermal properties of the samples. Background contributions to the signal were subtracted resulting in measurements of the apparent heat capacity $c_p(T)$.

SAXS. Small angle X-ray scattering experiments were carried out on a Kratky compact camera connected to a conventional X-ray tube, equipped with a focusing X-ray multilayer optics, a scanning scintillation detector and a temperature-controlled sample holder in which the sample was held in between aluminum foil. As the camera uses a slit focus, data were deconvoluted applying the desmearing algorithm by Strobl.[34] During the measurements, the sample chamber was evacuated.

WAXS. Wide angle X-ray scattering measurements were performed on a Siemens D5000 powder diffractometer in reflection geometry ($\theta-2\theta$, Rowland circle) equipped with a heatable sample support plate (HTK 1200, Anton Paar, Austria). The sample holder consisting of a silicon base plate and a copper frame was mounted on the heatable plate and kept in N_2-atmosphere during the measurement. For both SAXS and WAXS Cu K_α radiation was used (λ = 1.54 Å). For a precise analysis the angular scale of the diffractometer was calibrated by comparison with the SAXS scale using the (100) Bragg reflection of P3HT, which was visible in both setups.

AFM. Atomic force microscopy was performed with a Nanowizard from JPK Instruments (Berlin, Germany) using silicon cantilevers from Nanoworld with a nominal resonance frequency of 320 kHz and a stiffness of about 42 N/m. The instrument was operated in intermittent contact mode under ambient conditions.

Chemical Characterization. ^{1}H NMR spectra were recorded on a Bruker DRX 500 spectrometer at 500 MHz in chloroform solution. Size exclusion chromatography SEC measurements were carried out in THF using a UV detector from Waters and a mixed-C PL-Gel (PL) column. Polystyrene was used for calibration and 1,2-dichlorobenzene as an internal standard. MALDI−TOF MS measurements were performed on a Bruker Daltonic Reflex TOF using dithranol as matrix and a mixture of 1000:1 (matrix:polymer). The laser intensity was set to around 70%.

Samples. *Synthesis and Chemical Characterization.* Regioregular Poly(3-hexylthiophene) (P3HT) samples were synthesized using the Grignard metathesis polymerization (GRIM) developed by McCullough and co-workers.[35] The basic characteristics such as molecular weight, polydispersity and chain length are given in Table 1. The molecular weights and the polydispersities were determined by size exclusion chromatography (SEC) using polystyrene as external standard for calibration. The results are shown

Table 1. Molecular Characteristics of Samples Used in This Study[a]

sample	P3HT 3	P3HT 6	P3HT 12	C.S.
M_n (SEC) in kDa	5.2	7.9	18.5	20.0
M_w (SEC) in kDa	6.0	10.1	21.6	48.3
M_n by MALDI in kDa	3.2	6.6	12.4	
no. of repeating units (thiophene rings)	20	39	74	
calculated contour length in nm	7.7	14.9	28.3	
PDI (SEC)	1.15	1.28	1.16	2.41
% regioregularity (NMR)	97	97	97	94

[a] The contour length was calculated as the product of the number of repeating units times half of the lattice parameter c determined below. Note that M_w of the sample C.S. is considerably higher than that of sample P3HT 12.

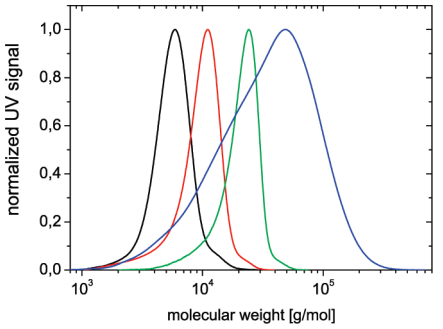

Figure 2. Molecular weight distribution of the P3HT samples under study as measured by size exclusion chromatography (black, P3HT 3; red, P3HT 6; green, P3HT 12; blue, C.S.).

in Figure 2. Since the hydrodynamic radii of rather stiff conjugated polymers like poly(3-hexylthiophenes) are larger than for polystyrene the molecular weight values are overestimated.[36] The peak maximum of the molecular weight distribution measured by SEC is about twice the number-average molecular weight determined on an absolute scale by MALDI−TOF MS, matrix-assisted laser desorption/ionization mass spectroscopy with time-of-flight detection (for $M \approx 5000-20000$ g/mol). These latter values were used to determine the degree of polymerization, i.e. the number of repeating units, and the contour length. For the synthetic method used, the first two units are coupled tail−tail,[37] while otherwise the number of irregular defects within the chain is very low and even hard to detect quantitatively by NMR. In general the regioregularity can be calculated from the NMR peaks for the four different triads TT−HH (7.05 ppm), TT−HT (7.00 ppm), HT−HH (7.02 ppm), and HT−HT (6.98 ppm).[38,39] Therefore, the range between 7.06 and 7.01 ppm for irregular couplings was integrated and compared to the range for the regioregular HT−HT couplings. The TT−HT (7.00 ppm) coupling could not be separated from the regioregular peak at 6.98 ppm even with a 500 MHz NMR. Thus, the given regioregularity takes into account only the defects within the chains, the tail−tail coupling from the starting unit is not included. For comparison, data from a commercial sample, obtained from Aldrich, have been included. Measurements on this sample were already published.[25] MALDI−TOF MS could not be carried out for this sample due to its large molecular weight and large polydispersity. The polymers are named according to their MALDI−TOF MS molecular weight and C.S. indicates commercial sample.

Sample Preparation. For the DSC measurements, P3HT flakes obtained from synthesis were used without any further treatment. Aluminum pans were filled with a mass of about 10 mg. To prepare homogeneous isotropic bulk samples for WAXS and SAXS, the materials were put into the respective holder (transmission geometry for SAXS, reflection geometry for WAXS), placed in an oven with nitrogen atmosphere, heated to the melt state and then cooled down slowly to room temperature. Films for AFM were spin coated with 2000 rpm from 0.3 to 0.5 wt % chloroform solution onto silicon wafers covered with a natural oxide layer. Subsequently, the films were heated in nitrogen atmosphere above their respective melting temperatures and cooled down slowly to room temperature.

Results and Discussion

Crystal Structure−Temperature Dependence. *Sequence of Phases with Temperature*. As described in the introduction P3HT exhibits a hierarchical structure which covers several length scales and comprises $\pi-\pi$ stacking, separation between main and side chains, and a semicrystalline morphology consisting of lamellar crystals and amorphous interlayers. To investigate the temperature dependence of this complex structure in detail we selected the sample with the lowest molecular weight (P3HT 3). It shows most clearly the phenomena which we think are general. A first overview can be gained from the DSC measurement shown in Figure 3.

There are four transitions from low to high temperatures. A small step in specific heat capacity, c_p around −10 °C indicates the glass transition of the amorphous part of the sample. The value of T_g is comparable to the glass transition temperature observed in regiorandom P3HT.[25] Consistently we find a reversible phase transition around 50−60 °C. As we will show below using X-ray scattering experiments, this transition can be attributed to side chain melting. While this attribution was presumed before,[23] it has to our knowledge not been proven by direct structural evidence as, e.g., by X-ray scattering. The reason might be that generally thermal properties of P3AT's depend strongly on the length of the side chains, on the molecular weight, and on the details of the

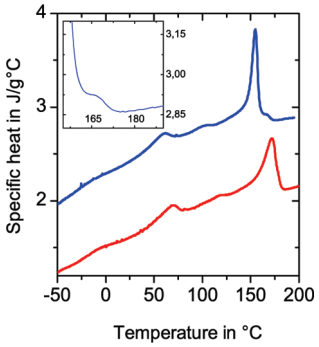

Figure 3. DSC heating (red) and cooling (blue, vertically shifted) curves of P3HT 3 measured with a rate of 20 K/min. The inset shows an enlarged part of the crystallization peak measured during cooling.

chemical structure. For these reasons, experimental results reported in the literature vary corresponding to advances in the synthesis of well-defined polymers. Correspondingly some temperature dependent structural changes have been observed in this intermediate temperature range,[14] but no clear reversible phase transition. As we will show also in our samples the transition is difficult to observe for higher molecular weights. The next peak around 170 °C is related to crystal melting. In the cooling run, a shoulder on the high temperature side can be recognized (cf. inset), suggesting that melting and crystallization occurs in two steps, namely over an intermediate layered mesophase of smectic symmetry,[25] as it is consistent with the scattering experiments shown below. For the slight bump in the DSC signal around 125 °C, we did not find any corresponding structural changes.

To find out what kind of structural changes take place at the transitions observed in DSC, we performed temperature dependent SAXS and WAXS measurements as shown in Figure 4. The Bragg peaks visible in WAXS for intermediate temperatures (above 60 °C) correspond to the typical pattern usually reported for room temperature measurements of commercial P3HT (cf., e.g., ref 25). For the sample P3HT 3 in the low temperature phase, additional reflections showed up, indicating that the transition at 60° is related to structural changes in the crystalline part of the sample. Details will be discussed below. Measurements taken during a cooling run (not shown) confirmed that the changes in the scattering pattern were reversible. A comparison of the data obtained at 140, 160, and 180 °C shows that melting occurs in two steps. At 160 °C, all Bragg reflections but the first (peak 1), which reflects the layered structure resulting from a separation between main and side chains, have disappeared. Only the next measurement taken at 180 °C corresponds to a completely amorphous sample giving rise to diffuse scattering only, without Bragg reflections. The SAXS data are consistent with the occurrence of a two-step melting process. They show two peaks, namely again peak 1 discussed above and peak 0 at $q \approx 0.065$ Å^{-1} which is caused by stacks of alternating lamellar crystals and amorphous layers with a periodicity $d_1 = 2\pi/q \approx 9.7$ nm. In an intermediate temperature range ($T = 170-180$ °C) peak 1 is still observable, while peak 0 has already disappeared; i.e., there is an intermediate layered structure of separated main and side chains but without lamellar crystals. As it can be noticed from the fact that the smectic phase is still observable at 180 °C in SAXS and not in WAXS, there are slight deviations in the temperature calibration between the two instruments. This does not affect the overall result.

Crystal Structure at Room Temperature. A close inspection of the WAXS profiles in Figure 4 reveals that above the

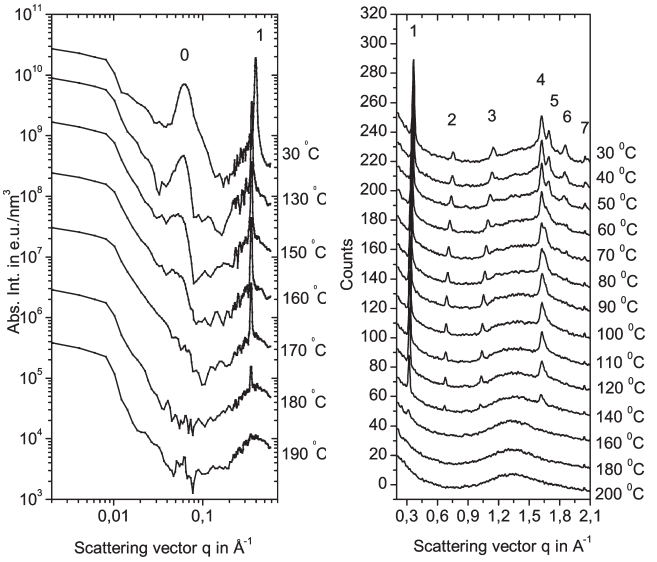

Figure 4. Temperature dependent small angle (left) and wide angle (right) X-ray powder scattering profiles of P3HT 3 reflecting the semicrystalline morphology and the crystal structure (cf. Figure 1). All data were taken during heating. Bragg reflections are numbered from low to high scattering vector. Peak 7 contains a contribution which comes from the substrate and remains therefore visible up to the highest temperatures. The temperatures at which the transitions occur differ slightly between the two series of measurements due to temperature calibration errors, mainly in the WAXS chamber.

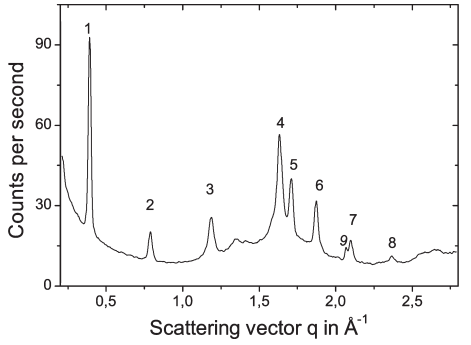

Figure 5. Powder diffraction profile of P3HT 3 measured at room temperature. Bragg reflections are numbered from low to high scattering vector. Peak 9 originates from the sample holder.

transition at about 60 °C peaks 5, 6, and 7 disappear. In order to understand the corresponding structural changes, it is necessary to index the additional Bragg reflections of the low temperature phase. Figure 5 shows a WAXS scattering profile measured at room temperature with better statistics and a broader q-range than in Figure 4. While powder diffraction profiles of P3HT have been reported many times in the literature, such detailed diffraction patterns as in Figure 5 are rare and were more often measured on thin films.[15,16] In general scattering patterns of P3HT could be explained based on the orthorhombic unit cell originally proposed by Prosa et al.[13,14] A second structure with reduced main-chain side-chain layer distance was also reported in the literature,[40] but the additional features appearing in our samples relate to the lateral packing of the chains. In our case we could not explain the positions of the higher order reflections with an orthorhombic unit cell, but satisfactory agreement between calculated and measured positions of the reflections could be obtained using the monoclinic structure proposed by Brinkmann and Rannou.[15] The corresponding analysis is shown in Table 2.

Table 2. Proposed Indices of the Bragg Reflections Visible in Figure 5[a]

peak	(*hkl*)	$2\theta_B$ [deg]	q [Å^{-1}]	q_{calc} [Å^{-1}]	d [Å]
1	100	5.61	0.399		15.73
2	200	11.20	0.796	0.80	
3	300	16.84	1.19	1.20	
4	020/002	23.20	1.64		7.66
5	120	24.28	1.72	1.71	
6	220	26.63	1.88	1.86	
7	320	29.90	2.11	2.08	
8	420	33.83	2.37	2.35	

[a] Bragg angles $2\theta_B$ were calibrated by comparison with the corresponding position of the (100) peak in the SAXS measurement. q_{calc} is the value of the scattering vector q_{hkl} calculated from a monoclinic unite cell with lattice cell parameters $\boldsymbol{a}$, $\boldsymbol{b}$, $\boldsymbol{c}$ determined from reflections 1 and 4, and $\gamma = 93°$ as proposed by Brinkmann.

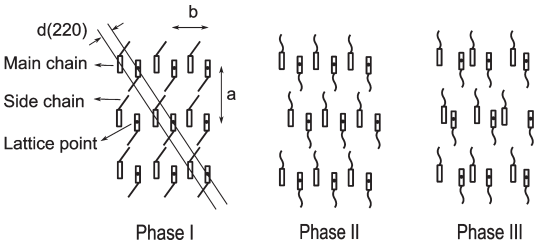

Figure 6. Schematic illustration of structure and order in the different phases of P3HT. (220) planes are indicated. (viewing direction along c). Phase I: regular 3D-crystal with ordered main and side chains. Phase II: regular packing of the main chains only. The side chains are molten and disordered; correspondingly different main chain layers lose correlation with each other (schematically shown for the central layer). Phase III: liquid-like packing of main and side chains, but the separation between main and side chains still exists.

The first three peaks 1−3 shown in the X-ray diffraction profile in Figure 5 can be identified as series of (h00) reflections. We used the (100) reflection to calibrate the angular scale of the diffractometer, the fact that q_{200} and q_{300} were close to the expected values confirms the validity of this procedure. As shown by Tashiro,[14] peak 4 is a superposition of the (020) and a weak (002) reflection. Having identified these first four reflections the lattice parameters could be determined as $a = 15.73$ Å, $b = 7.66$ Å, $c = 7.66$ Å for P3HT 3. Compared to the values in the literature, our lattice parameters are slightly smaller.[14,15,25] Starting from these values we could consistently attribute the indices (120), (220), (320), and (420) to the remaining reflections 5, 6, 7, and 8, as the corresponding data in Table 2 show.

Obviously, the peaks disappearing at the phase transition around 60 °C have all mixed indices, i.e. $h \neq 0 \wedge k \neq 0$. The corresponding lattice planes connect different layers of main chains (or side chains) and therefore require registry in the a- and b- direction of the chain positions in different layers. This is only possible if the side chains are in an ordered state, we therefore attribute the disappearance of the additional peaks to a loss of order in the side chains, i.e., side chain melting. Above this transition the material exhibits a peculiar state of order. In one direction there is a regular periodic stack of alternating side chains and main chains, and the main chains within the layers are arranged on a regular 2D lattice. But this arrangement is uncorrelated between different layers, as the side chains separating different layers are disordered and probably at least in the outer part very mobile. Figure 6 illustrates this point schematically.

Side Chain Packing in Room Temperature Phase. The exact conformation and packing of the side chains in P3HT has been under discussion for a long time. Recently it was

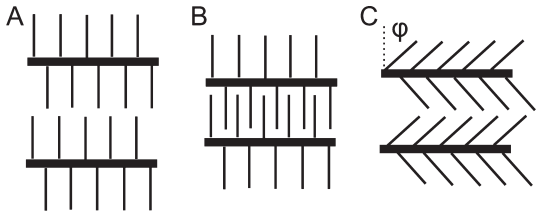

Figure 7. Schemes of possible types of side chains packing. Key: (A) noninterdigitated, nontilted; (B) interdigitated, nontilted; (C) noninterdigitated, tilted.

concluded from a detailed study on a P3HT with higher molecular weight that the side chains are disordered.[19] Given that we have strong evidence for an ordered arrangement of the side chains in the low temperature phase, namely the registry between different layers, we tried to explore the consequences for the packing of side chains similarly as in ref 19. Basically there are three possibilities discussed in the literature, all schematically depicted in Figure 7. It is the question if the chains interdigitate and if they are tilted with respect to the normal of the $b-c$ plane. We assume as a basic presupposition that the lateral packing density of the hexyl side chains ρ_{ch} in the side chain layers must be similar as in polyethylene (PE) or alkane crystals. The corresponding value reflects the intermolecular interaction potential between neighboring $(CH_2)_n$ chains in all-trans conformation. For PE $\rho_{ch,PE} \approx 5.44\ \mathrm{nm}^{-2}$, corresponding to two chains per orthorhombic unit cell with lattice parameters $a = 7.42$ Å and $b = 4.95$ Å. Starting with the assumption of noninterdigitating, nontilted side chains, the corresponding value for P3HT amounts to only about 2/3 of this value, $\rho_{ch,P3HT} \approx 3.41\ \mathrm{nm}^{-2}$ (2 side chains per unit cell with lattice parameters $\boldsymbol{b} = 7.66$ Å, $\boldsymbol{c} = 7.66$ Å). For interdigitating chains this value would increase by a factor of 2, $\rho_{ch,P3HT} \approx 6.82\ \mathrm{nm}^{-2}$, i.e. about 25% higher than in PE. Tilting the side chains leads to increasing values of $\rho_{ch,P3HT}$ by a factor $\cos \varphi^{-1}$, with ϕ being the angle between side chain axis and the normal of the $b-c$ plane, i.e.

$$\varphi \approx \arccos \frac{3.41\ \mathrm{nm}^{-2}}{5.42\ \mathrm{nm}^{-2}} \approx 51.0^{\circ}$$

Taking molecular dimensions into account, this value is compatible with the measured value of the lattice parameter a.

Comparison with Higher Molecular Weights. The observation of the phase transition around 60 °C and the highly ordered crystal structure at room temperature are essential for the structural scheme summarized in Figure 6. As this transition was not clearly observed before in other P3HT materials the question arises how general our results are. On the basis of some additional evidence presented below we think that the phase scheme above is indeed general, but that the phase transition is kinetically hindered for higher molecular weights.

Figure 8 shows a comparison of three DSC heating measurements on P3HT 12, one taken directly after cooling, one after two months of storage at room temperature, and the third corresponding to the first heating of the pristine sample as obtained. While during heating directly after cooling the transition at 60 °C could not be detected, the latter two samples clearly showed a peak indicative of the phase transition. Establishing the correlation between the main chain layers is obviously a slow process for high molecular weight materials; i.e., the phase transition is kinetically hindered. However, the equilibrium state for the high molecular weight sample seems to be the same as for the low molecular weight sample.

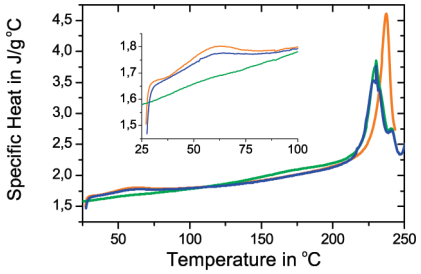

Figure 8. DSC measurements of sample P3HT 12: directly after cooling from the melt (green), after annealing for 2 months at room temperature (blue), and first heating of pristine sample as obtained (orange). The inset shows the range around the phase transition around 60 °C in more detail. For the high molecular weight samples, the phase transition appears only after prolonged storage time at room temperature.

Semicrystalline Morphology. We now turn our attention to the larger scale structure, the semicrystalline morphology. In the crystalline state, oligomers and polymers generally adopt a stretched, often helical conformation and form thin lamellar crystals. For higher molecular weight chain folding sets in. The crystals are separated by amorphous layers consisting of noncrystallizable end groups, folds, or other topological defects. It has been shown that basically the same phenomena happen for the somewhat stiffer P3HT chains.[15,24] The materials under study here with their high chemical regularity are of course no exception, as it can be easily visualized by scanning force microscopy (AFM).

Exemplary AFM phase images of P3HT thin films on silicon are shown in Figure 9. For such samples, after heating above the respective melting temperature and subsequent slow cooling the a-direction is typically oriented perpendicular to the substrate;[25] i.e., in the images the $b-c$ plane is visible, showing the typical pattern of lamellar or fibrillar crystals. AFM phase contrast is related to the Fourier transform of the interaction force between tip and sample during approach and penetration of the sample.[41] As the corresponding height images do not show the same pattern and as the surface of the film is chemically uniform, it is obvious that the phase signal reflects mainly the different mechanical properties of crystalline and amorphous parts of the sample. For a sample with hard−soft contrast generally higher values of the phase correspond to the stiffer material.[41] Clearly with increasing molecular weight the thickness of the crystals increased and the arrangement of the crystals became somewhat less well ordered. A direct quantitative determination of the thicknesses of the crystals and the amorphous layers is difficult due to resolution problems.

We tried to correlate these observations to a more quantitative analysis based on DSC and SAXS measurements. Figure 10 shows DSC measurements of all three P3HT samples under study. Additionally a measurement of the commercial sample is shown, data on this sample were already published by Hugger et al.[25] As already mentioned the phase transition related to side chain melting disappears for the higher molecular weight, but also the transition from the crystalline state to the melt changes. The melting temperature as well as the latent heat of melting increases with increasing molecular weight. The increase of the melting temperature can be explained by the increase of lamellar thickness with increasing molecular weight. This effect is normally well described by the Gibbs−Thomson equation

$$T_m(d) = T_m^{\infty}\left(1 - \frac{2\sigma}{\Delta h}\frac{1}{d}\right)$$

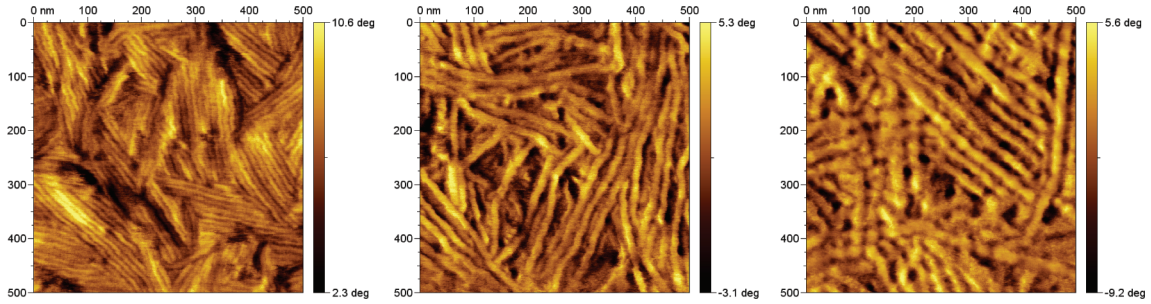

Figure 9. Intermittent contact mode AFM phase images of thin P3HT films of different molecular weight (from left to right: P3HT 3, P3HT 6, P3HT 12).

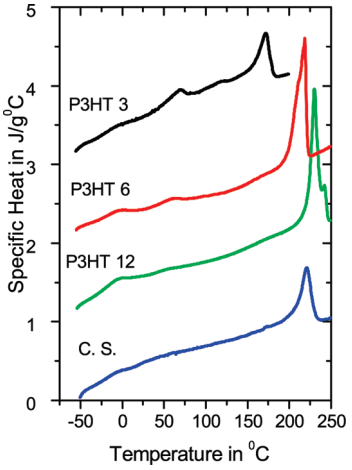

Figure 10. DSC heating curves for all samples (heating rate = 20 K/min, C.S., P3HT 6, P3HT 3 vertically shifted by −1, 1, 2 J/g °C, respectively, with P3HT 12 not shifted).

giving the melting temperature of a lamellar crystal of thickness d. Here T_m^∞ is the equilibrium melting temperature, σ the surface energy, Δh the heat of melting per volume for a 100% crystalline material, and d the thickness of the lamellar crystal.[5] The observed melting point depression is therefore consistent with the AFM observations. The fact that also ΔH is higher for the samples P3HT6 and P3HT12 indicates that not only the crystal thickness but also the crystallinity increases for higher molecular weight; i.e., the thickness of the amorphous layers does not increase in the same way as the crystalline layers. The results of a quantitative analysis of the DSC measurements are given in Table 3. Here the integration for the determination of ΔH comprises the full transition from the crystalline state over the layered phase to the isotropic melt (not for sample C.S.). It is interesting to note that obviously these two transitions (crystalline to layered and layered to isotropic) are both affected by the molecular weight. For the second transition from the layered to the isotropic state this effect is obviously not caused by crystal thickness. If we understand the ordered, layered state as a result of the separation between main and side chains, it is clear that the degree of polymerization of the main chain enters the free energy balance, because $n = Nm$ CH_2 units participate in the demixing (N-degree of polymerization, m-number of alkyl units in side chains per monomer). In this context, it is worthwhile to compare the results obtained for the commercial sample. While the molecular weight is substantially higher, the values for melting temperature and the heat of melting are comparable or lower than for the sample P3HT 12. Obviously neither the crystal thickness nor the crystallinity increases further with molecular weight. Most likely this effect is dominantly caused by the lower

Table 3. Quantitative Analysis of DSC and SAXS Measurements on P3HT Samples of Different Molecular Weights

sample	P3HT 3	P3HT 6	P3HT 12	C. S.
no. of repeating units	20	39	74	
calculated contour length in nm	7.7	14.9	28.3	
		DSC		
ΔH_m in J/g	11.3	21.1	22.4	14.7
T-range of integration in °C	110−186	150−228	170−248	160−237
T_m(peak) in °C	172	216	230	221
T_m(onset) in °C	154	200	223	208
		SAXS		
long period d_l in nm	9.2	14.8	27.0	

regioregularity of C.S. . Additional contributions from the higher polydispersity of C.S. might also contribute. It is well-known that chemical defects or counits which cannot be built into the crystal structure strongly limit the crystallinity as well as the crystal thickness in semicrystalline polymers. The phase transition from the layered structure to the melt on the other hand is shifted toward higher temperatures outside the range of the measurement,[25] as this transition is obviously not as strongly affected by regioregularity.

To get more direct quantitative information about the semicrystalline morphology we performed SAXS measurements of the samples P3HT 3, 6, and 12. The data are shown in Figure 11. All three data sets show a peak indicating a periodic arrangement of lamellar crystals. The peak position allows to determine the average long period d_l of the lamellar stack. As the intensity at higher q is masked by the peak from the (100) reflection, a more quantitative analysis giving d_a and d_c separately[42] was not successful. Nevertheless already a comparison of the long period and the contour length is instructive. For P3HT 3 d_l is larger than the contour length, while for the higher molecular weight samples the two values are comparable. This result gives a hint to what causes the small crystallinity of P3HT 3 which is somewhat unexpected, taking into account that normally oligomers form extended chain crystals with very high crystallinity. Although the direct comparison of contour length and long period does not take into account the additional space needed for the side chains, it certainly shows that P3HT 3 forms extended chain crystals. But obviously there is a layer of noncrystallizable material on both sides of the crystals as it is schematically illustrated in Figure 12. In this morphology one end of every chain is not built into the crystal, taking into account the tail-to-tail coupling of the first two units as well as polydispersity effects. Clearly this effect will be present also for higher molecular weights but show up most strongly for P3HT 3. In conclusion P3HT 3, 6, and 12 dominantly form extended

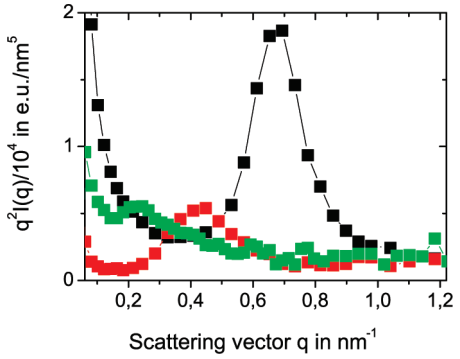

Figure 11. Lorentz corrected SAXS scattering intensity $I(q)q^2$ vs q. The peak position corresponds to the inverse long period $2\pi/d_l$ (black, P3HT 3; red, P3HT 6; green, P3HT 12).

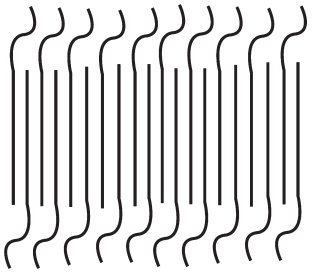

Figure 12. Scheme of lamellar crystal with amorphous layer containing noncrystallizable end groups. The rounded shape of the chains outside the crystals stands for a nonstretched, amorphous conformation, which is of course in reality not the same for all chains.

chain crystals covered by an amorphous layer of decreasing relative weight for the higher molecular weight materials. Additionally partial chain folding might set in for higher molecular weight, but this is certainly not yet a strong effect in the molecular weight range of our samples.

Conclusions and Outlook

Our measurements demonstrate that by studying a chemically very well-defined P3HT series structural features of the material can be observed which are otherwise hidden and difficult to detect. Using DSC, SAXS, and WAXS for a P3HT with low molecular weight, we were able to determine the temperature dependent phase diagram. There are strong indications that with increasing temperature the following order of structures is general for P3HT: 3D-crystal with ordered main and side chains; regular packing of the main chains in 2D with disordered side-chains; layered structure of separated main and side chains with liquid like packing within the layers; isotropic liquid. For higher molecular weights the first transition at 60 °C, which happens at a temperature relevant for photovoltaic applications, seems to be kinetically hindered. This points to the importance of long time annealing effects. All materials studied are semicrystalline, and the crystallinity increases with molecular weight. While it is unusual that polymers of modest molecular weight, forming extended chain crystals, contain an appreciable fraction of amorphous material, it here has to be taken into account that for synthetic reasons chain ends show a different coupling of the 3-hexylthiophene units and cannot be included into the crystals. This effect becomes less important for higher molecular weights. For the crystallization conditions and samples studied we do not observe strong indications for chain folding. What remains open at this point is a quantitative value for the crystallinity of our samples. It would require a detailed analysis of the scattering pattern in order to separate amorphous and crystalline contributions to the WAXS pattern. Qualitatively the results suggest a crystallinity somewhat below 50% for P3HT3. This estimate questions the often used value for ΔH of 99 J/g deduced in literature from a DSC analysis of crystallization of P3HT in solution.[23] On the basis of this value, we would estimate a crystallinity of only about 10% for P3HT 3, which is hard to reconcile with the qualitative features of the powder WAXS pattern.

Concerning the relation between molecular weight, structure and morphology on one hand and charge transport properties on the other hand, we can draw general conclusions from this work. Certainly P3HT is a complex material, for which the molecular weight, the exact chemical microstructure as well as the thermal history determine structure and morphology. Therefore, one should probably distinguish between fractionated material and polymers resulting from a controlled polymerization as the molecular weight distribution can be still largely different. Furthermore, it is difficult to conclude on the crystallinity from measurements based on thin film samples alone. A well ordered surface pattern does not necessarily mean high crystallinity and X-ray intensities might be strongly affected by orientation effects. Another comment concerns the way how thin films are prepared. In order to determine inherent material properties it is in our view advantageous to look in a first instance at equilibrium structures. The morphology resulting from a process like spin coating or drop casting will in most cases not correspond to equilibrium and will therefore depend on kinetic factors, too. An annealing step is only expected to lead to equilibrium if the annealing temperature is high enough to ensure sufficient molecular mobility, which will often be related to the phase transition temperature of the corresponding ordering process. Additionally in thin films there might be orientation induced by interfacial interactions or confinement which is important as the electronic properties of P3HT are anisotropic.[43,44]

Acknowledgment. We thank M. Beiner for helpful discussions about side chain packing, I. Gunkel for complementary SAXS measurements, C. Eisenschmidt for help with the WAXS measurements and K. Herfurt for technical help with DSC measurements. Furthermore, T.T.-A. is grateful to W. deJeu for previous discussions about scattering analysis of side chain melting. This work was supported by the DFG—German Science Foundation (SPP 1355) and the state Sachsen-Anhalt. R.L. acknowledges BayEFG for a stipend and the "ENB-Macromolecular Science" study program.

References and Notes

(1) Kim, Y.; Cook, S.; Tuladhar, S.; Choulis, S.; Nelson, J.; Durrant, J.; Bradley, D.; Giles, M.; Mcculloch, I.; Ha, C.; Ree, M. *Nat. Mater.* **2006**, *5*, 197.
(2) Li, G.; Shrotriya, V.; Huang, J.; Yao, Y.; Moriarty, T.; Emery, K.; Yang, Y. *Nat. Mater.* **2005**, *4*, 864.
(3) Kroon, R.; Lenes, M.; Hummelen, J. C.; Blom, P.W. M.; De Boer, B. *Polym. Rev.* **2008**, *48*, 531.
(4) Forrest, S. *Nature* **2004**, *428*, 911.
(5) Strobl, G. *The physics of polymers: Concepts for understanding their structures and behavior*, 3rd ed.; Springer: Berlin and Heidelberg, Germany, 2007.
(6) Bao, Z.; Dodabalapur, A.; Lovinger, A. J. *Appl. Phys. Lett.* **1996**, *69*, 4108.
(7) Ong, B. S.; Wu, Y.; Li, Y.; Liu, P.; Pan, H. *Chem.—Eur. J.* **2008**, *14*, 4766.
(8) DeLongchamp, D. M.; Kline, R. J.; Jung, Y.; Germack, D. S.; Lin, E. K.; Moad, A. J.; Richter, L. J.; Toney, M. F.; Heeney, M.; McCulloch, I. *ACS Nano* **2009**, *3*, 780.
(9) Heffner, G. W.; Pearson, D. S. *Macromolecules* **1991**, *24*, 6295.
(10) Jiang, X. M.; Österbacka, R.; Korovyanko, O.; An, C. P.; Horovitz, B.; Janssen, R. A. J.; Vardeny, Z. V. *Adv. Funct. Mater.* **2002**, *12*, 587.
(11) Winokur, M. J.; Spiegel, D.; Kim, Y. H.; Hotta, S.; Heeger, A. J. *Synth. Met.* **1989**, *28*, 419.

(12) Mccullough, R. D.; Tristramnagle, S.; Williams, W. P.; Lowe, R. D.; Jayaraman, M. *J. Am. Chem. Soc.* **1993**, *115*, 4910.
(13) Prosa, T. J.; Winokur, M. J.; Moulton, J.; Smith, P.; Heegert, A. J. *Macromolecules* **1992**, *25*, 4364.
(14) Tashiro, K.; Ono, K.; Minagawa, Y.; Kobayashi, M.; Kawai, T.; Yoshino, K. *J. Pol. Sci. Part B: Polym. Phys.* **1991**, *29*, 1223.
(15) Brinkmann, M.; Rannou, P. *Adv. Funct. Mater.* **2007**, *17*, 101.
(16) Joshi, S.; Grigorian, S.; Pietsch, U. *Adv. Funct. Mater.* **2002**, *12*, 587.
(17) Yamamoto, T.; Komarudin, D.; Arai, M.; Lee, B.-L.; Suganuma, H.; Asakawa, N.; Inoue, Y.; Kubota, K.; Sasaki, S.; Fukuda, T.; Matsuda, H. *J. Am. Chem. Soc.* **1998**, *120*, 2047.
(18) Mena-Osteritz, E.; Meyer, A.; Langeveld-Voss, B. M. W.; Jassen, R. A. J.; Meijer, E. W.; Baeuerle, P. *Angew. Chem., Int. Ed.* **2000**, *39*, 2679.
(19) Kline, R. J.; DeLongchamp, D. M.; Fischer, D. A.; Lin, E. K.; Richter, L. J.; Chabinyc, M. L.; Toney, M. F.; Heeney, M.; McCulloch, I. *Macromolecules* **2007**, *40*, 7960.
(20) Park, K. C.; Levon, K. *Macromolecules* **1997**, *30*, 3175.
(21) Liu, S. L.; Chung, T. S. *Polymer* **2000**, *41*, 2781.
(22) Causin, V.; Marega, C.; Marigo, A.; Valentini, L.; Kenny, J. M. *Macromolecules* **2005**, *38*, 409.
(23) Malik, S.; Nandi, A. *J. Polym. Sci., Part B: Polym. Phys.* **2002**, *40*, 2073.
(24) Brinkmann, M.; Wittmann, J.-C. *Adv. Mater.* **2006**, *18*, 860.
(25) Hugger, S.; Thomann, R.; Heinzel, T.; Thurn-Albrecht, T. *Colloid Polym. Sci.* **2004**, *282*, 932.
(26) Street, R. *Nat. Mater.* **2006**, *5*, 171.
(27) Kline, R.; McGehee, M.; Kadnikova, E.; Liu, J.; Frechet, J. *Adv. Mater.* **2003**, *15*, 1519.
(28) Kline, R. J.; McGehee, M. D. *Macromolecules* **2005**, *38*, 3312.
(29) Verilhac, J.-M.; LeBlevennec, G.; Djurado, D.; Rieutord, F.; Chouiki, M.; Travers, J.-P.; Pron, A. *Synth. Met.* **2006**, *156*, 815.
(30) Zhang, R.; McCullough, R. D. *J. Am. Chem. Soc.* **2006**, *128*, 3480.
(31) Zen, A.; Pflaum, J.; Hirschmann, S.; Zhuang, W.; Jaiser, F.; Asawapirom, U.; Rabe, J.; Scherf, U.; Neher, D. *Adv. Funct. Mater.* **2004**, *14*, 757.
(32) Zen, A.; Saphiannikova, M.; Neher, D.; Grenzer, J.; Grigorian, S.; Pietsch, U.; Asawapirom, U.; Janietz, S.; Scherf, U.; Lieberwirth, I.; Wegner, G. *Macromolecules* **2006**, *39*, 2162.
(33) Brinkmann, M.; Rannou, P. *Macromolecules* **2009**, *42*, 1125.
(34) Strobl, G. R. *Acta Crystallogr.* **1970**, *A26*, 367.
(35) Sheina, E. E.; Liu, J.; adn D. W. Laird, M. C. I.; McCullough, R. D. *Macromolecules* **2004**, *37*, 3526.
(36) Holdcroft, S. *J. Polym. Sci., Part B: Polym. Phys.* **1991**, *29*, 1585.
(37) Miyakoshi, R.; Yokoyama, A.; Yokozawa, T. *J. Am. Chem. Soc.* **2005**, *127*, 17542.
(38) Chen, T.; Rieke, R. D. *J. Am. Chem. Soc.* **1992**, *114*, 10088.
(39) Barbarella, G.; Bongini, A.; Zambianchi, M. *Macromolcules* **1994**, *27*, 3039.
(40) Prosa, T. J.; Winokur, M. J.; McCullough, R. D. *Macromolecules* **1996**, *29*, 3654.
(41) Schröter, K.; Petzold, A.; Henze, T.; Thurn-Albrecht, T. *Macromolcules* **2009**, *42*, 1114.
(42) Albrecht, T.; Strobl, G. *Macromolecules* **1995**, *28*, 5827.
(43) Yang, H.; LeFevre, S. W.; Ryu, C. Y.; Bao, Z. *Appl. Phys. Lett.* **2007**, *90*, 172116.
(44) Kline, J.; McGehee, M.; Toney, M. F. *Nat. Mater.* **2006**, *5*, 222.